Photomineralization of terrigenous dissolved organic matter in Arctic coastal waters from 1979 to 2003: Interannual variability and implications of climate change

Simon Belanger, Huixiang Xie, Nickolay Krotkov, Pierre Larouche, Warwick F. Vincent, Marcel Babin

Photomineralization of terrigenous dissolved organic matter in Arctic coastal waters from 1979 to 2003: Interannual variability and implications of climate change

Simon Bélanger,[1,2] Huixiang Xie,[3] Nickolay Krotkov,[4] Pierre Larouche,[5] Warwick F. Vincent,[6] and Marcel Babin[1,2]

Received 16 February 2006; revised 7 June 2006; accepted 28 June 2006; published 7 November 2006.

[1] Photomineralization of terrigenous dissolved organic matter (tDOM) in the Arctic Ocean is limited by persistent sea ice cover that reduces the amount of ultraviolet (UV) radiation reaching the underlying water column. UV-dependent processes are likely to accelerate as a result of shrinking sea ice extent and decreasing ice thickness caused by climatic warming over this region. In this study, we made the first quantitative estimates of photomineralization of tDOM in a coastal Arctic ecosystem under current and future sea ice regimes. We used an optical-photochemical coupled model incorporating water column optics and experimental measurements of photoproduction of dissolved inorganic carbon (DIC), the main carbon product of DOM photochemistry. Apparent quantum yields of DIC photoproduction were determined on water samples from the Mackenzie River estuary, the Mackenzie Shelf, and Amundsen Gulf. UV irradiances just below the sea surface were estimated by combining satellite backscattered and passive microwave radiance measurements with a radiative transfer model. The mean annual DIC photoproduction between 1979 and 2003 was estimated as 66.5 ± 18.5 Gg carbon in the surface waters of the southeastern Beaufort Sea, where UV absorption is dominated by chromophoric dissolved organic matter discharged by the Mackenzie River. This value is equivalent to 10% of bacterial respiration rates, 8% of new primary production rates and 2.8 ± 0.6% of the 1.3 Tg of dissolved organic carbon (DOC) discharged annually by the Mackenzie River into the area. During periods of reduced ice cover such as 1998, the latter value could rise to 5.1% of the annual riverine DOC discharge. Under an ice-free scenario, the model predicted that 150.5 Gg of DIC would be photochemically produced, mineralizing 6.2% of the DOC input from the Mackenzie River. These results show that the predicted trend of ongoing contraction of sea ice cover will greatly accelerate the photomineralization of tDOM in Arctic surface waters.

Citation: Bélanger, S., H. Xie, N. Krotkov, P. Larouche, W. F. Vincent, and M. Babin (2006), Photomineralization of terrigenous dissolved organic matter in Arctic coastal waters from 1979 to 2003: Interannual variability and implications of climate change, *Global Biogeochem. Cycles*, *20*, GB4005, doi:10.1029/2006GB002708.

1. Introduction

[2] Terrigenous dissolved organic matter (tDOM) is an abundant component of Arctic polar surface waters [see *Benner et al.*, 2005, and references therein] as a result of the large amounts of riverine tDOM that enter the Arctic Ocean relative to its volume [*Aagaard and Carmack*, 1989]. The refractory character of tDOM, as observed in several Arctic marginal seas [e.g., *Dittmar and Kattner*, 2003; *Meon and Amon*, 2004], may also contribute to the high concentrations of Arctic Ocean tDOM. Recent studies suggest that slightly more than 50% of the annual input of terrigenous dissolved organic carbon (tDOC) to the Arctic Ocean is remineralized before its transport to the North Atlantic [*Hansell et al.*, 2004]. However, quantitative information on major tDOM loss processes in the Arctic is still lacking.

[3] There is growing evidence indicating a major role of photooxidation in the remineralization of tDOM in the coastal oceanic environment [e.g., *Benner and Opsahl*, 2001; *Hernes and Benner*, 2003; *Kieber et al.*, 1990]. Other studies suggested that a large fraction of the marine plankton-

[1]Laboratoire d'océanographie de Villefranche, Université Pierre et Marie Curie-Paris, Villefranche-sur-Mer, France.
[2]Also at Laboratoire d'océanographie de Villefranche, CNRS, Villefranche-sur-Mer, France.
[3]Institut des Sciences de la Mer de Rimouski, Université du Québec à Rimouski, Rimouski, Quebec, Canada.
[4]Goddard Earth Sciences and Technology Center, University of Maryland Baltimore County, Baltimore, Maryland, USA.
[5]Institut Maurice-Lamontagne, Pêches et Océans Canada, Mont-Joli, Quebec, Canada.
[6]Département de Biologie and Centre d'Études Nordiques, Université Laval, Quebec City, Quebec, Canada.

0886-6236/06/2006GB002708

derived dissolved organic carbon (DOC) pool also can be photochemically mineralized in the open ocean [*Johannessen*, 2000; *Johannessen and Miller*, 2001]. Although there is molecular evidence that photochemical transformation of tDOM occurs in the Arctic Ocean [*Benner et al.*, 2005], this mechanism is not considered of importance because of the prevailing low solar angle, cloudy conditions and permanent sea ice cover [*Amon and Meon*, 2004; *Benner et al.*, 2004]. Sea ice and its overlying snow cover is known to be a strong attenuator of ultraviolet (UV) radiation in both polar regions [*Vincent and Belzile*, 2003].

[4] Recent observations in the Arctic reveal that sea ice conditions are changing, with a 20% decrease in the summer areal extent of sea ice over the last 3 decades [e.g., *Cavalieri et al.*, 2003]. In addition, the thinning of sea ice has also been observed in several parts of the Arctic Ocean [e.g., *Wadhams and Davis*, 2000], permitting more UV radiation to reach the water column. Moreover, a complete loss of summer ice is predicted for later this century [*Arctic Climate Impact Assessment*, 2005]. In parallel, a decrease in stratospheric ozone concentration (O_3), which results in an increase of UVB (280–320 nm) radiation at sea surface, was recently reported over the high northern latitudes [*Fioletov et al.*, 2004; *Rex et al.*, 2004]. These observations suggest that the amount of photochemically active UV radiation 280–400 nm penetrating into the Arctic waters could have significantly increased in the last decades, and that this effect may accelerate in the coming years.

[5] In addition to alteration in sea ice dynamics, a number of other recent observations suggest that the Arctic is currently experiencing rapid and extensive environmental changes in response to global climate warming [*Overland et al.*, 2004; *Serreze et al.*, 2000]. Arctic rivers account for about 10% of global terrestrial organic carbon export to the ocean [*Rachold et al.*, 2004]. This percentage is likely to increase markedly during the next century [*Frey and Smith*, 2005] as a result of increasing river discharge [*Peterson et al.*, 2002] and thawing of the permafrost [*Camill*, 2005]. The latter stores one third of the global soil carbon and contains 7 to 26% of all terrestrial organic carbon stored since the Last Glacial Maximum [*Smith et al.*, 2004]. To assess and predict the impact of climate change on the marine carbon cycle, it is critical to determine the transformation and fate of the exported terrestrial carbon, including photochemical production of dissolved inorganic carbon (DIC), which is the main carbon product of chromophoric DOM (CDOM) photochemistry [*Miller and Zepp*, 1995; *Mopper and Keiber*, 2002].

[6] The objectives of this study are to assess the present significance of photooxidation of CDOM in the tDOM cycling in ice-free Arctic seawaters, and to assess the potential impact of the reduction of sea ice extent on the removal of tDOM through this process. Our field study was conducted in the Canadian Shelf of the Beaufort Sea where a large amount of tDOM is discharged by the Mackenzie River (Figure 1). In terms of dissolved organic carbon export, the Mackenzie River is the fourth largest among the Arctic rivers, discharging ~1.3 Tg of tDOC per year [*Telang et al.*, 1991]. This large tDOC flux explains the high concentration of terrestrial CDOM found in the entire Western Arctic Ocean [*Guay et al.*, 1999; *Guéguen et al.*, 2005]. As this area has experienced a significant decrease in sea ice areal extent between 1979 and 2000 [*Barber and Hanesiak*, 2004], photooxidation may have become a significant component of the tDOM cycling in this Arctic coastal ecosystem. In this study, experimentally determined wavelength-specific apparent quantum yields (AQY) of DIC production, along with remote sensing–derived spectral irradiances (300 to 600 nm) and surface areas of open waters, were used to model the depth-integrated photochemical production rates of DIC in the ice-free waters of the southeastern Beaufort Sea. To assess recent trends in the DIC production, we calculated the annual photochemical production of DIC for the period 1979 to 2003.

2. Materials and Methods

2.1. Sample Collection and Storage

[7] Sampling was conducted in June and July 2004 onboard the CCGS *Amundsen* in the Mackenzie Shelf, the Gulf of Amundsen, and the Arctic Canada basin (Figure 1) as part of the Canadian Arctic Shelf Exchange Study (CASES) program, and onboard the CCGS *Nahidik* in the Mackenzie River estuary in late July during the Arctic River-Delta Experiment (ARDEX). Surface water samples were collected at 79 locations during CASES (Figure 1) for measurement of the absorption coefficients of CDOM (a_{CDOM}) and suspended particles (a_p). The samples were filtered through 0.2-μm Anotop® syringe filters (Whatman) and collected into 100-mL acid-cleaned amber glass bottles. Suspended particles were retained by 25-mm GF/F glass fiber filters (Whatman) by filtering 0.1 to 3.5 L of seawater. The glass bottles and GF/F filters were stored frozen (seawater: −20°C; particles: −80°C) in the dark until being analyzed ~4 months later in the land-based laboratory at Rimouski (a_{CDOM}) and Villefranche-sur-mer (a_p).

[8] Six stations were sampled for determination of the apparent quantum yield (AQY) spectra of DIC photoproduction: two in the Mackenzie River estuary, one on the Mackenzie Shelf (ARDEX cruise), and three in the Amundsen Gulf (CASES cruise) (Figure 1 and Table 1). Surface water (~5 m deep) in the Amundsen Gulf was taken with Teflon-coated Niskin bottles and gravity-filtered through a Pall AcroPak 1000 Capsule sequentially containing 0.8-μm and 0.2-μm polyethersulfone membrane filters. During the ARDEX cruise, surface water was collected using an acid-cleaned plastic bucket and transferred to acid-cleaned carboys. Both the bucket and carboys were profusely rinsed three times with sample water. The surface water was then filtered through sequential 3-μm and 0.2-μm pore size polysulfone filters (PALL corporation). All filtered samples were stored cold (4°C) in the dark in acid-cleaned 4-L clear glass bottles and shipped to the laboratory at Rimouski.

2.2. Optical Measurements

[9] The frozen seawater samples were thawed and warmed to room temperature. Their optical densities (OD), referenced to pure water, were measured in a 10-cm quartz cuvette between 250 and 800 nm with 1-nm increments

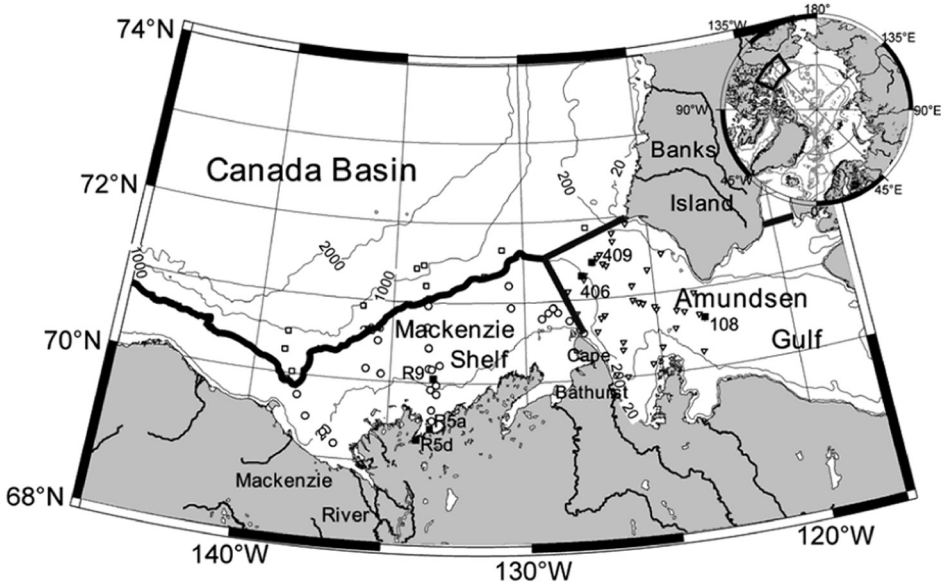

Figure 1. Location of CASES stations sampled for absorption measurements in 2004 over the Mackenzie Shelf (open circles), in the Amundsen Gulf (open triangles), and in the Canada Basin (open squares). ARDEX and CASES samples collected for ϕ_{DIC} determination are shown as closed squares.

using a Perkin-Elmer Lambda 35 dual beam spectrophotometer. A background correction was applied by subtracting the absorbance value averaged over an interval of 5 nm around 685 nm from all the spectral values [*Babin et al.*, 2003]. The spectral absorption coefficient of CDOM, $a_{CDOM}(\lambda)$ (m^{-1}), was calculated as

$$a_{CDOM}(\lambda) = \frac{2.303\ OD(\lambda)}{l}, \quad (1)$$

where l is the optical path length (0.1 m). Note that $a_{CDOM}(\lambda)$ spectra of frozen samples were lower in magnitude ($\sim$10%) than the refrigerated samples used for irradiation experiments.

[10] The spectral absorption coefficients of the particles retained on the GF/F filters, $a_p(\lambda)$ (m^{-1}), were determined at 1-nm resolution between 350 and 750 nm according to the transmittance-reflectance technique described by *Tassan and Ferrari* [1995] using a Perkin-Elmer Lamda-19 spectrophotometer equipped with a 60-mm integrating sphere. Before the measurements of the OD, the frozen filters were hydrated with 1–2 mL of filtered seawater and warmed to room temperature to avoid phytoplankton cell lysis. The OD of particles on filter, obtained by subtracting the mean OD of 10 hydrated blank GF/F filters at each wavelength from the total measured OD with the reference beam in air, was converted to a_p using the expressions given by *Tassan and Ferrari* [2002]. Assuming that particle absorption is negligible in the near-IR [*Babin and Stramski*, 2002], $a_p(750)$ was subtracted from a_p at all wavelengths <750 nm.

2.3. Irradiation Experiments

[11] The irradiation setup and procedure for determining the AQY of DIC production, ϕ_{DIC} (mol C (mol photons)$^{-1}$), were similar to those adopted by *Johannessen and Miller* [2001]. Briefly, stored samples were refiltered through 0.2-μm polycarbonate membrane filters (Millipore), acidified with HCl to pH $\sim$3 and purged with CO_2-free air for $\sim$24 hours to reduce the background DIC to undetectable levels. The purging gas was humidified (100% relative humidity) so that no net loss of water occurred owing to evaporation. The DIC-free water samples were buffered back to approximately the original pH values with powdered sodium borate (ACS grade) and transferred into precombusted (420°C), gas-tight quartz-windowed cylindrical cells (internal diameter: 0.02 m; length: 0.14 m) and irradiated in a

Table 1. Chemical and Physical Properties of Samples Used for the ϕ_{DIC} Determinations

Station-Mission	Date of Sampling	Latitude, °N	Longitude, °W	Depth, m	S	T, °C
R5d-ARDEX	31-07	69.28	133.97	0	1.57	16.1
R5a-ARDEX	31-07	69.42	133.5	0	8.19	12.2
R9-ARDEX	28-07	70.05	133.42	0	25.81	9.23
108-CASES	07-06	70.63	123.22	10	30.09	−1.08
406-CASES	16-06	71.30	127.75	5	30.77	0.51
409-CASES	23-07	71.46	127.3	5	28.79	3.46

thermostated incubator (0 ± 0.5°C) using a SUNTEST CPS solar simulator equipped with a 1-kW Xe lamp. Eight spectral treatments were examined employing successive Schott long-pass glass filters; the Schott numbers of these filters are WG280, WG295, WG305, WG320, WG345, GG395, GG435 and GG495. Spectral irradiance under each filter was measured with an Optronics OL-754 UV-vis spectroradiometer fitted with a fibreoptic cable. The irradiance level under the WG280 filter was set to 190 W m^{-2} for stations R5a, R5d and R9, and to 585 W m^{-2} for stations 108, 406 and 409, and the irradiation time varied from 24.5 to 46 hours, depending on the abundance of CDOM in the irradiated samples (Figure S1 in auxiliary materials[1]). The rationale for choosing these irradiation times and light intensities was to obtain measurable DIC while minimizing the extent of photobleaching. Parallel incubations in the dark were conducted to correct for potential nonphotochemical production of DIC. Extreme caution was taken to minimize bacterial contamination during sample handling and transfer. Small increases of DIC in the dark controls were often observed, but they were always similar to or less than the amounts of DIC formed in the quartz cell under the GG495 filter. The dark control values were subtracted during the calculation of DIC photoproduction in each irradiated vessel.

2.4. DIC Measurement and Calculation of ϕ_{DIC}

[12] After irradiation, 1.50 mL of sample (in triplicates) were mixed with 1 mL of 10% DIC-free H_3PO_4 in an acid trap and purged with ultra-high-purity nitrogen. DIC in the sample was converted into CO_2 which was introduced by a nitrogen carrier stream to a LI-COR 6262 CO_2/H_2O analyzer for quantification. The whole system was calibrated immediately before and after sample measurement with varying volumes (usually 0.20, 0.40, 0.60, and 0.8 mL) of a 12-μM DIC standard. This working standard was daily prepared by diluting a 600-μM sodium carbonate stock solution; the stock solution was made by dissolving dried sodium carbonate (Na_2CO_3, BDH AnalaR) in DIC-free pure water. All calibration curves resulted in $R^2 > 0.999$. The analytical precision was determined to be ~2% at a concentration of 4 μM DIC.

[13] The spectral apparent quantum yield of DIC production, $\phi_{DIC}(\lambda)$, was defined as the moles of DIC photochemically produced per mole of photons absorbed by CDOM at wavelength λ. To derive the $\phi_{DIC}(\lambda)$ values, the iterative curve-fitting method of *Johannessen and Miller* [2001] was applied. Briefly, this method assumes an appropriate mathematical functional form with unknown parameters to express the change of ϕ_{DIC} as a function of wavelength. Decreasing exponential functional forms are usually chosen for photochemical quantum yield spectra. The amount of DIC produced in an irradiation cell over the exposure time can then be predicted as a product of three terms: the assumed $\phi_{DIC}(\lambda)$ functional form, the measured incident irradiance, and the sample absorption coefficient. The optimum values of the unknown parameters in the assumed $\phi_{DIC}(\lambda)$ functional form are obtained by varying these parameters from initial estimates until minimum difference between the measured and predicted DIC production is achieved. The absorption coefficient was measured before and after irradiation and was averaged according to first-order decay kinetics, which well describe photobleaching [*Del Vecchio and Blough*, 2002; *Xie et al.*, 2004]. We followed the recommendation of *Hu et al.* [2002] for the calculation of the number of photons absorbed by CDOM and adopted the following modified exponential form to fit the data:

$$\phi_{DIC}(\lambda) = k_1 e^{k_2/(\lambda+k_3)}, \quad (2)$$

where k_1, k_2 and k_3 are fitting parameters.

2.5. Modeling DIC Photoproduction

[14] Assuming that the seawater optical properties are vertically constant in the photic zone and that the flux of photons backscattered to the atmosphere is negligible, the daily depth-integrated DIC photoproduction rate, P_{DIC} (mol C m^{-2} d^{-1}), can be calculated as

$$P_{DIC} = \int_{\lambda=300}^{600} E_d(0^-, \lambda) \frac{a_{CDOM}(\lambda)}{a_t(\lambda)} \phi_{DIC}(\lambda) d\lambda, \quad (3)$$

where $a_t(\lambda)$ (m^{-1}) is the total absorption coefficient (i.e., sum of absorption by seawater, CDOM and particles) and $E_d(0^-, \lambda)$ (mol photons m^{-2} d^{-1}) is the spectral daily downward irradiance just beneath sea surface. Equation (3) was used to calculate the temporal changes in P_{DIC} in different regions of the Beaufort Sea over the period between 1979 and 2003. Constant regional values of $a_{CDOM}(\lambda)/a_t(\lambda)$ and $\phi_{DIC}(\lambda)$ determined from our field and laboratory work were assumed (see below). Note that in the open ocean where the fraction of light absorbed by the CDOM (i.e., the ratio $a_{CDOM}(\lambda)/a_t(\lambda)$) approaches the value of 1 in the UV domain, P_{DIC} can be approximated by integrating the product of $E_d(0^-, \lambda)$ and $\phi_{DIC}(\lambda)$ over λ [e.g., *Johannessen*, 2000]. When particles compete for light absorption in the UV domain, as in coastal waters, the parameter $a_{CDOM}(\lambda)/a_t(\lambda)$ of equation (3) is necessary to avoid overestimation of P_{DIC}.

[15] By using constant regional value for $\phi_{DIC}(\lambda)$, our approach did not explicitly take into account any potential dependence on light dose of this quantity; i.e., the effect of CDOM light history on $\phi_{DIC}(\lambda)$. *Johannessen and Miller* [2001] observed a 2.3 times increase in the $\phi_{DIC}(\lambda)$ after a coastal water sample was extensively photobleached (loss of absorbance in the UV wavelengths > 50%) while *Vähätalo and Wetzel* [2004] found a 13% decrease in the DOC loss AQY of a lake water sample with a 9% increase in the photons absorbed by CDOM. Therefore both the direction and magnitude of change in photomineralization AQY in response to light dose remain unclear. In the present study, significant photobleaching was incurred during the AQY experiments (Figure S1 in auxiliary materials) while no appreciable photobleaching seemed to have taken place during the transport of CDOM from the estuary of the Mackenzie River to the Shelf or even further seaward (see

[1] Auxiliary material data sets are available at ftp://ftp.agu.org/apend/gb/2006gb002708. Other auxiliary material files are in the HTML.

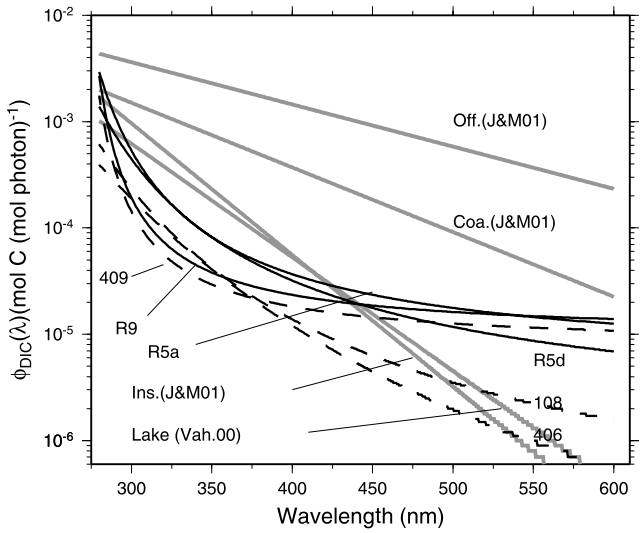

Figure 2. The ϕ_{DIC} spectra determined on water samples collected during ARDEX (R5a, R5d, and R9; solid thin lines) and CASES (108, 406 and 409; dashed thin lines). The grey curves are the average ϕ_{DIC} spectra published by *Vähätalo et al.* [2000] for a boreal lake, and by *Johannessen and Miller* [2001] for inshore, coastal and offshore waters.

section 3). Ideally, experimentally determined AQYs only apply to timescales over which the amount and spectral quality of the light absorbed by CDOM in the field are equivalent to those of the light absorbed by CDOM in irradiation experiments. On larger geochemically significant timescales (e.g., the residence times of the Mackenzie River's runoff in the Canada Basin or the entire Arctic Ocean), the uncertainties in the calculation of P_{DIC} associated with the dose dependence of $\phi_{DIC}(\lambda)$ should be smaller, since the extent of photobleaching in the field on these timescales, as compared to the timescales of land-to-sea CDOM transport, are likely closer to that occurring in our laboratory irradiations.

[16] The spectral daily downward irradiance received at the sea surface was calculated using a radiative transfer method that uses as inputs satellite measurements of total atmospheric ozone column content and of cloud cover derived from Total Ozone Mapping Spectrometer (TOMS) data [*Herman et al.*, 1999; *Krotkov et al.*, 2002, 1998, 2001]. The calculations were made for each day between February 1979 to April 1993, and between August 1996 to November 2001, which correspond to the periods when TOMS data were available. Calculations were done for conditions with and without cloud cover. The method was modified in two respects. First, instead of using the monthly minimum Lambertian equivalent reflectivity (MLER) for the surface albedo (A_s) from climatology, we used a linear combination of albedos for open water and sea ice,

$$A_s = A_{water}(1 - SIC) + A_{ice}SIC \quad (4)$$

where *SIC* is the fractional sea ice surface concentration (dimensionless, from 0 to 1), and A_{water} and A_{ice} are the water and sea ice albedos, respectively. Note that A_s must be accounted for in the calculation of $E_d(\lambda)$ because multiple scattering between sea surface and atmosphere can be significant in the UV domain. Daily *SIC* data were obtained from the National Snow and Ice Data Center (NSIDC) and were derived from observations of the Scanning Multi channel Microwave Radiometer (SMMR; 1979–1987) or Special Sensor Microwave Imager (SSM/I; 1987–2003) using the NASA Team algorithm [*Cavalieri et al.*, 1990]. The values for A_{water} (0.05) and A_{ice} (0.76) were adopted from the MLER climatology for summer (*SIC* = 0) and winter (*SIC* = 1) seasons, respectively, published by *Herman and Celarier* [1997] and *Herman et al.* [1999]. Second, the calculations of irradiance were spectrally extended to cover the range from 300 to 600 nm (with 0.5-nm resolution). As the above procedure yields downward irradiance just above sea surface, we applied a factor of 0.95 to account for specular reflection and to obtain $E_d(0^-, \lambda)$ just beneath surface as needed in equation (3).

[17] For the calculation of total DIC photoproduction, the Southeastern Beaufort Sea was divided into three subregions: the Mackenzie Shelf (MS; 80 000 km^2; depth < 200 m; west of Cape Bathurst), the Amundsen Gulf (AG; 87 000 km^2; >118°W) and the Canada Basin (CB; 240 000 km^2; <145°W; <74°N) (Figure 1). The area of open water (in km^2) in each subregion was calculated daily as the sum of the products of the term (1-*SIC*) and the grid

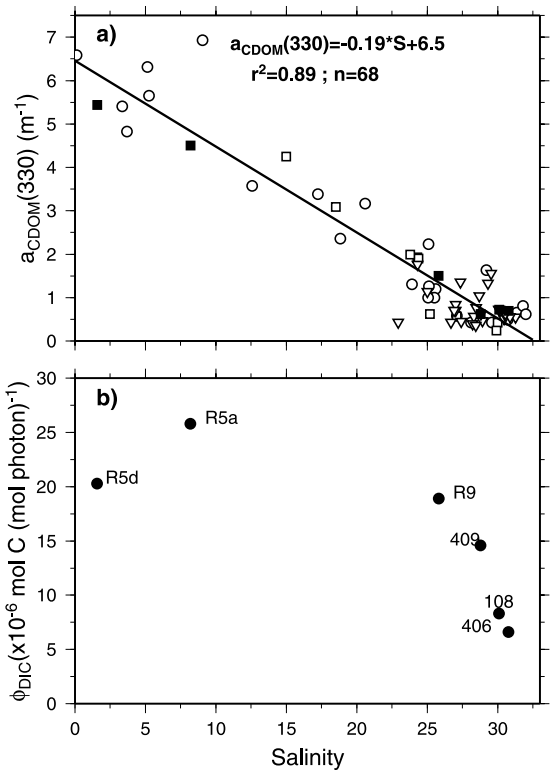

Figure 3. (a) Variation of $a_{CDOM}(330)$ with salinity for water samples collected in the MS (open circles), the AG (open triangles), the CB (open squares). Samples collected for ϕ_{DIC} determination are shown as closed squares. (b) Variation of the weighted quantum yield normalized to the integrated irradiance, $\overline{\phi_{DIC}}$, with salinity.

Table 2. CDOM Properties and Model Parameters for ϕ_{DIC}

Station	$a_{CDOM}330$, m^{-1}	S_{CDOM}[a]	$\phi_{DIC}(\lambda) = k_1 e^{k_2/(\lambda+k_3)}$				
			k_1	k_2	k_3	r^{2}[b]	$\overline{\phi_{DIC}}$ ($\times 10^{-6}$)
R5d	5.44	0.0190	1.2×10^{-6}	726	−176	0.998	20.3
R5a	4.50	0.0201	4.9×10^{-6}	352	−224	1.00	25.8
R9	1.50	0.0204	9.6×10^{-6}	128	−257	0.984	18.9
108	0.72	0.0200	2.7×10^{-10}	5232	88.7	0.976	8.8
406	0.69	0.0191	6.7×10^{-8}	1538	−111	0.996	6.6
409	0.62	0.0217	7.44×10^{-6}	128	−256	0.994	14.6

[a]Spectral slope of the the model $a_{CDOM}(\lambda) = a_{CDOM}(\lambda_0)e^{S_{CDOM}*(\lambda_0-\lambda)}$.
[b]The correlation coefficient (r^2) is from the linear regression between modeled and measured DIC production.

area of each grid cell falling into that subregion. The total daily DIC photoproduction of a region was obtained by multiplying the area of open water in that region by P_{DIC}. For the Mackenzie Shelf, P_{DIC} was calculated using the average ϕ_{DIC} determined on water samples collected from stations R5a, R5d and R9 (Figure 1). Since station 108 was sampled right in the middle of the Amundsen Gulf, the $\phi_{DIC}(\lambda)$ spectrum for this location was used to calculate P_{DIC} in the AG. As no AQY samples were taken from the Canada Basin, we assumed the $\phi_{DIC}(\lambda)$ spectra for stations 406 and 409 to be representative of the CB area. This assumption is based on the facts that these two stations are in the vicinity of the CB, and that most surface waters entering the AG come from the CB [*Carmack and Macdonald*, 2002], although these two stations could be influenced to some extent by the Mackenzie River's runoff. It should be noted that our regional DIC photoproduction was calculated using the daily estimates of $E_d(\lambda)$, except for days when TOMS data were lacking (i.e., from April 1993 to August 1996, and after November 2001). For those days, an averaged $E_d(\lambda)$ value calculated over the period of TOMS data availability was used to estimate the P_{DIC}.

3. Results and Discussion

3.1. Apparent Quantum Yield for DIC Photoproduction

[18] The six ϕ_{DIC} spectra determined during this study are shown in Figure 2 and the parameters of the quasi-exponential model (equation (2)) are given in Table 2. The exponential form adopted here has a steeper slope and fits better the measured production ($r^2 > 0.97$) than the two-parameter single exponential form used by *Johannessen and Miller* [2001] and *Vähätalo et al.* [2000]. A detailed comparison between these two functional forms is provided in the supplementary online material. To compare the photoreactivity of the CDOM, we calculated the mean ϕ_{DIC} value weighted by an incident solar irradiance spectrum,

$$\overline{\phi_{DIC}} = \frac{\int_{280}^{600} E_d(0^-,\lambda)\phi_{DIC}(\lambda)d\lambda}{\int_{280}^{600} E_d(0^-,\lambda)d\lambda}. \quad (5)$$

Here E_d (0^-, λ) was modeled using the Tropospheric Ultraviolet Visible (TUV) model [*Madronich and Flocke*, 1999] for summer solstice at 70°N with clear sky, moderate aerosols concentration (optical thickness at 550 nm of 0.1), and total ozone column content of 330 DU. Note that only the spectral shape of E_d (0^-, λ) influenced the value of $\overline{\phi_{DIC}}$ (e.g., for a total ozone column content of 480 DU, the difference in $\overline{\phi_{DIC}}$ is <2%). The rationale for this normalization is to reduce the ϕ_{DIC} spectrum to a single value that accounts for the shapes of both the ϕ_{DIC} and E_d (0^-, λ) spectra, thereby giving more weight to the wavelengths at which photooxidation is maximal (i.e., 320–340 nm). The $\overline{\phi_{DIC}}$ measured in this study varied from 6.6 to 25.8×10^{-6} mol C (mol photons)$^{-1}$ (Table 2). These values are lower than the $\overline{\phi_{DIC}}$ obtained by *Johannessen and Miller* [2001] for coastal ($31 < S < 35$) and offshore ($S > 35$) waters with 174.0 and 786.5×10^{-6} mol C (mol photons)$^{-1}$, respectively. However, our $\overline{\phi_{DIC}}$ values for low-salinity water samples (R5a and R5d, salinity <9) are comparable to the inshore ($S < 31$) value of 30.4×10^{-6} mol C (mol photons)$^{-1}$ measured by *Johannessen and Miller* [2001] and to the average $\overline{\phi_{DIC}}$ of 25.9 ×

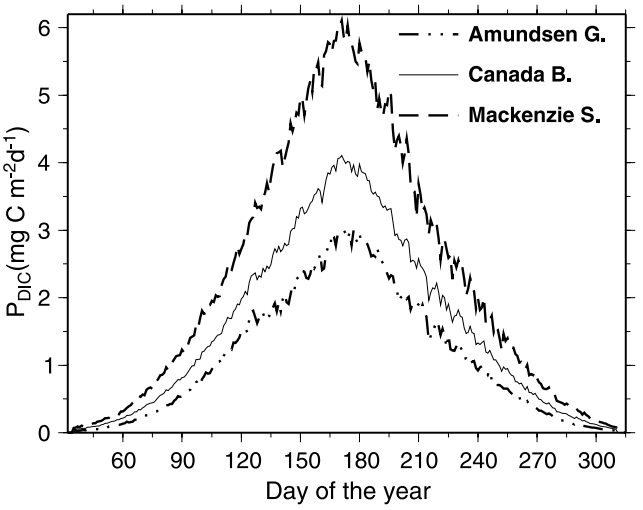

Figure 4. Average DIC photoproduction rates, P_{DIC}, calculated using the ϕ_{DIC} representing each subregion: R5a, R5d and R9 for the Mackenzie Shelf; 108 for the Amundsen Gulf; 406 and 409 for the Canada Basin.

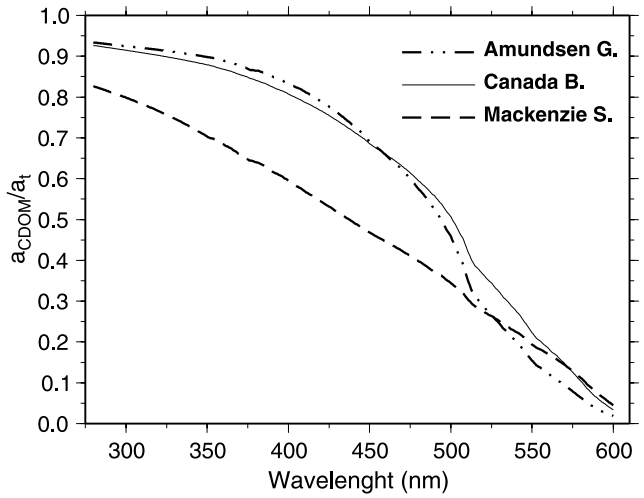

Figure 5. Average spectral light fraction absorbed by CDOM in the surface waters at stations (Figure 1) sampled over the Mackenzie Shelf (dashed line), in Amundsen Gulf (dash-dotted line), and in Canada Basin (thin line).

10^{-6} mol C (mol photons)$^{-1}$ reported by *Vähätalo et al.* [2000] for water samples from Valkea-Kotinen, a humic lake located in coniferous forest of Finland (61°14′N; 25°04′E). While CDOM was mixed conservatively over the shelf estuary, as suggested by the negative linear correlation between a_{CDOM} and salinity (Figure 3a), we observed a nonlinear decrease of ϕ_{DIC} with increasing salinity (Figure 3b). This behavior possibly resulted from a conservative mixing of high-ϕ_{DIC} inshore waters with low-ϕ_{DIC} offshore waters and a nonconservative changes in the photoreactivity of CDOM across the salinity gradient. The decrease of ϕ_{DIC} with salinity observed in this study is opposite to the trend observed by *Johannessen and Miller* [2001] who proposed that, as the terrestrial aromatic structures in terrestrial CDOM are eliminated by photobleaching or as marine-derived CDOM increasingly dominates the light absorption, the proportion of DIC-producing to non-DIC-producing chromophores in CDOM increases. In the present study, photochemical fading of terrestrial CDOM is not supported by the conservative behavior of $a_{CDOM}(\lambda)$ (Figure 3a). In contrast, the lower ϕ_{DIC} values were observed at stations 108 and 406 (S = 30–31) sampled in June and away from direct input of the Mackenzie River. Overall, Figure 3b suggests that the photoreactivity of tDOM drained into the Mackenzie River changed when it was mixed into coastal and offshore waters (S < 30), and/or that marine algae-derived DOM was less photoreactive than tDOM in terms of photoproduction of DIC. Because of the small number of ϕ_{DIC} observations, and the lack of chemical characterization of the whole CDOM pool, it is not possible to provide a clear interpretation of the behavior of the ϕ_{DIC} observed in this area.

3.2. Role of DIC Photoproduction in the Organic Carbon Cycling

[19] The yearly pattern of DIC photoproduction (P_{DIC}), averaged over the period corresponding to TOMS data availability (01/1979 to 04/1993; 08/1996 to 11/2001), is shown in Figure 4. At summer solstice, P_{DIC} reached 6.1, 2.9 and 4.1 mg C m^{-2} d^{-1} for MS, AG and CB, respectively. Given that the spectral irradiance was similar for each subregion, the difference in P_{DIC} was mainly due to regional differences in ϕ_{DIC} (Figure 2) and in the fraction of light absorbed by CDOM (Figure 5). While CDOM largely dominated the total light absorption at wavelengths <380 nm in CB and AG (>90%), the high concentration of particulate matter in the MS reduced light availability to CDOM by 10 to 20% compared with the other two subregions. Nevertheless, P_{DIC} was larger in the MS due to the higher ϕ_{DIC} in the intermediate salinity range (Figure 3b).

[20] To assess the importance of photomineralization relative to other biogeochemical processes affecting the marine carbon cycle, our DIC photoproduction rates were compared with published bacterial respiration and primary production data for the same areas. On the basis of leucine uptake rates, *Garneau et al.* [2006] reported low bacterial production rates of 12 to 112 μg C m^{-3} d^{-1} (mean: 48 μg C m^{-3} d^{-1}) in the fall of 2002 in the vicinity of the Mackenzie River estuary. Assuming a typical growth efficiency of 27% for coastal Arctic bacteria [*Meon and Amon*, 2004], the bacterial respiration rate would be ~3.2 mg C m^{-2} d^{-1} in the upper 25 m of the water column. For comparison, P_{DIC} was 0.6 mg C m^{-2} d^{-1} at that time of the year (Figure 4), equivalent to ~19% of the bacterial respiration. In late June and early July 2004, when primary productivity and temperature are higher, the bacterial respiration rate in the upper 25 m ranged from 20.2 to 77.8 mg C m^{-2} d^{-1} (mean: 49.0 mg C m^{-2} d^{-1}) on the shelf (M.-È. Garneau, unpublished data, 2006). During the same period, P_{DIC} in the MS was 5.1 mg C m^{-2} d^{-1} (Figure 4 and Table 3), equivalent to

Table 3. Comparison Between Daily DIC Photoproduction and Total and New Primary Production Rates in Open Water[a]

Subregion	Period	Primary Production		P_{DIC}
		Total	New	
Mackenzie Shelf (80 000 km^2)	late July	100–200[b]	67–134[b]	3.5–5.0
Canada Basin (240 000 km^2)	late August	79–145 (106)[c]	14–26 (19)[c]	1.3–1.8
Amundsen Gulf (87 000 km^2)	late August	91.9[c]	13.2[c]	1.0

[a]Units are mg C m^{-2} d^{-1}.
[b]From *Carmack et al.* [2004].
[c]From *Lee and Whitledge* [2005], personal communication of S. Lee for AG values.

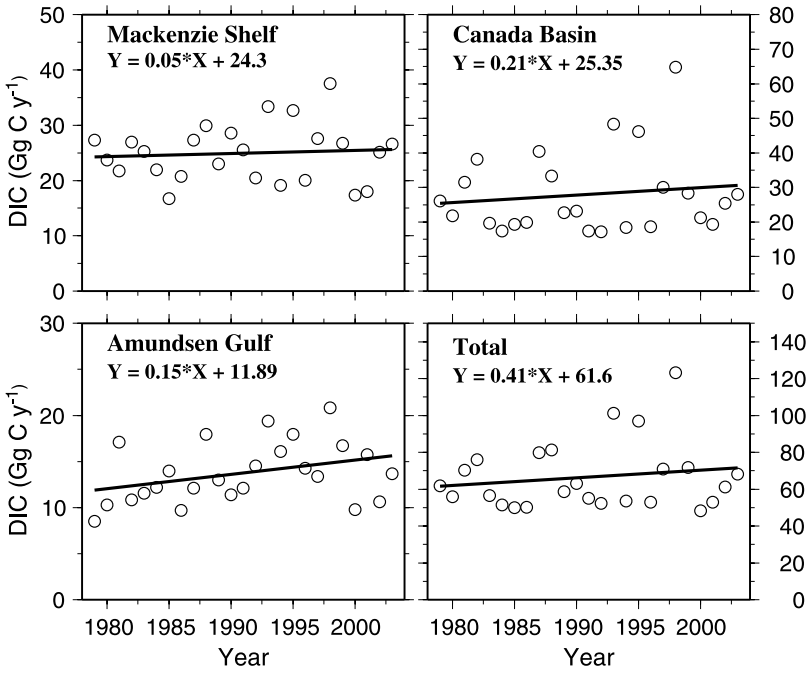

Figure 6. Trends in the annual DIC photoproduction for period 1979–2003 for the Mackenzie Shelf, the Amundsen Gulf, the Canada Basin, and the sums of the three subregions.

10.4% of the bacterial respiration.

[21] Table 3 compares our P_{DIC} values with recent published values of primary production (PP) and new production (in the sense of *Dugdale and Goering* [1967]) for open waters in the same areas. PP in the MS is typically 100 to 200 mg C m^{-2} d^{-1} in late July while new production (based on nitrate drawdown) is 67 to 134 mg C m^{-2} d^{-1} [*Carmack et al.*, 2004]. Values reported for late August in the Canada Basin range from 79 to 145 mg C m^{-2} d^{-1} for PP, with a mean of 106 mg C m^{-2} d^{-1}, and from 14 to 26 mg C m^{-2} d^{-1} for new production (based on nitrate and ammonium uptake), with a mean of 19 mg C m^{-2} d^{-1} [*Lee and Whitledge*, 2005]. In the AG, primary and new productions in late August 2002 were 91.9 and 13.2 mg C m^{-2} d^{-1}, respectively (S. H. Lee, personal communication, 2005). On the basis of our estimates of P_{DIC}, photomineralization of DOC occurs at a rate equivalent to 2.6–7.8, 6.8–9.4 and 7.6% of the amount of organic carbon produced by new production in MS, CB, and AG, respectively. Note that for the small area near the Cape Bathurst, however, satellite-based PP rates can reach up to 2800 mg C m^{-2} d^{-1} during the spring phytoplankton bloom [*Arrigo and van Dijken*, 2004]. Therefore the relative contribution of photomineralization to the organic carbon cycling could be much lower during short periods of bloom conditions.

3.3. Interannual Variability in DIC Photoproduction

[22] Figure 6 shows the annual photoproduction of DIC from 1979 to 2003. The mean annual production (±s.d.) was 24.9 ± 5.2, 13.7 ± 3.3 and 27.8 ± 11.8 Gg C in the MS, AG and CB, respectively. When all regions are pooled together, the photoproduction was on average 66.5 ± 18.4 Gg C yr^{-1}. Because of the large interannual variability, the positive slopes of the linear regressions between the production rate and time are not significantly different from zero. Nevertheless, the positive trends observed over the 25 years are higher for the AG and CB (+1.5 and +2.1 Gg C $decade^{-1}$, respectively) than for the MS (+0.5 Gg C $decade^{-1}$). On the basis of these trends, the DIC photoproduction increased by 5.0%, 26.3%, and 18.1% between 1979 and 2003 for the MS, AG, and CB, respectively, with an overall increase of 14.8%.

[23] The large interannual variability of the DIC photoproduction is mainly due to variability in sea ice cover. Figure 7 shows the strong positive correlation between the annual photoproduction of DIC and the average area of open water for each subregion. Note that the timing of the opening of sea ice is also important owing to the strong seasonal variability of P_{DIC} (Figure 4). For instance, the presence or absence of an ice cover in June has a stronger impact on the annual DIC photoproduction than it does in September. Figure 8 shows the changes in the number of days with open water (defined as >50% of the area free of ice) and in the date when the opening begins (i.e., first appearance of open water) for each subregion. The number of days with open water was on average (±s.d.) 116.8 ± 25.7, 125.7 ± 26.9 and 52.6 ± 47.6, and increased at a rate of 3.3, 12.0, and 9.3 days per decade for MS, AG and CB, respectively. Concurrently, the opening occurred on average at day 170.9 ± 20.3, 167.1 ± 18.9 and 181.6 ± 74.3, and decreased at rates of 1.9, 14.1 and 6.8 days per decade, for MS, AG and CB, respectively. As expected, we observed a larger interannual variability in sea ice concentration in the Canada Basin, which was due in part to the movement of

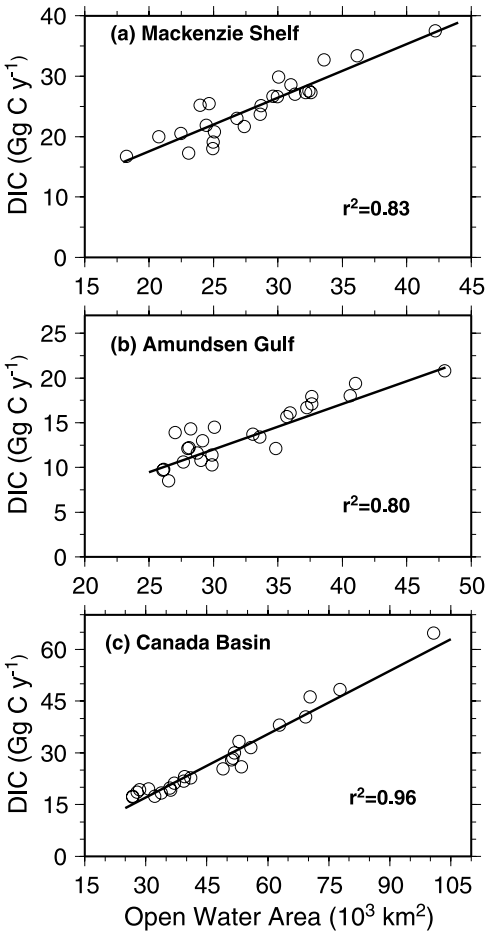

Figure 7. Correlation between the annual DIC photoproduction and the annual average area of open water for: (a) Mackenzie Shelf, DIC = 0.91×10^6 * X; (b) Amundsen Gulf, DIC = 0.52×10^6 * X; (c) Canada Basin, DIC = 0.63×10^6 * X. (X = open water area in km^2; slope in Gg C yr^{-1} km^{-2}; n = 25).

the Arctic central pack ice associated with dominant anticyclonic or cyclonic circulation regime [e.g., *Comiso et al.*, 2003]. For instance, the open-water area in the CB remained <50% during the summers of 1984, 1985, 1991, 1992 and 1996, while >120 days of fully open water were observed in 1987, 1993 and 1998.

[24] In addition to the variability in sea-ice cover and in the timing of its opening, the interannual variation of the atmospheric ozone concentration and cloud cover also contributed to the variability of DIC photoproduction. Figure 9 gives the trends between 1979 and 2001 in monthly averaged ozone column content as observed by TOMS over the southeast Beaufort Sea. In May, the ozone content was high and varied within a narrow range (379.5 ± 4.1 DU). In June and July, it decreased down to 322.4 ± 10.5 and 287.8 ± 7.22 DU, respectively. In August, the year-to-year variability was higher, as indicated by a higher standard deviation, 344.1 ± 37.2 DU, and a larger range, 270 to 400 DU. Linear regression gave a significant negative slope ($p < 0.05$) for July and August, −5.4 and −24 DU $decade^{-1}$, respectively. Nevertheless, the influence of the decreasing trends in the summer ozone column content on the DIC photoproduction was largely overshadowed by the variability in sea-ice cover (Figure 7).

[25] These results show that variation of sea-ice cover is the most important factor controlling the photochemical production of DIC in the Arctic surface waters. Our calculations did not account for seasonal variability in ϕ_{DIC} and optical properties of surface waters since they are unknown. Fortunately, our field sampling took place at the time of year (June and July) when both irradiance and river plume extent were maximal, and therefore when photooxidation processes were most intense. Our sampling time, however, might not adequately capture the influence of particulate matter dynamics on the availability of light to CDOM photochemistry. For instance, the continental shelf was sampled in early July, shortly after the ice breakup when the particle-rich river plume was spread over most of the shelf area [*Carmack and Macdonald*, 2002]. Later in the season the river discharge and suspended particulate matter abundance decrease sharply, allowing more light available for photochemical processes. The P_{DIC} for the MS, based on the ratio of a_{CDOM}/a_t obtained in early July, might therefore be underestimated for late summer. In contrast, spring bloom events, as observed in the area of Cape Bathurst polynya [*Arrigo and van Dijken*, 2004], could temporarily decrease a_{CDOM}/a_t in some areas.

[26] The trend in sea-ice cover extent observed in the southeastern Beaufort Sea is coherent with the trend observed over the whole Arctic Ocean [e.g., *Cavalieri et al.*, 2003; *Rothrock and Zhang*, 2005]. The rate of change in the northern hemisphere sea-ice cover extent between 1979 and 2002 was estimated to be $-0.36 \pm 0.05 \times 10^6$ km^2 $decade^{-1}$ [*Cavalieri et al.*, 2003]. If the P_{DIC} calculated in this study is applicable to the rest of the Arctic Ocean, the increase in DIC production since 1979 can be estimated for the whole Arctic. Using the area-normalized slope (in g C yr^{-1} km^{-2}) for the CB (Figure 7), we estimated that photochemical production of DIC in the northern hemisphere increased by 19.6–26.0 Gg C yr^{-1} between 1979 and 2002.

3.4. Implications for tDOC Cycling in Arctic Coastal Waters

[27] Physical transport appears the main mechanism responsible for the removal of tDOC in the Arctic Ocean. *Benner et al.* [2005] reported that physical transport of tDOC to the northeast Atlantic Ocean represents 25 to 33% of the 25 Tg tDOC yr^{-1} input into the Arctic Ocean. In addition, a similar fraction of tDOC may be exported through the Canadian archipelago into the northwest Atlantic [*Amon*, 2004] and into the Arctic deep basin resulting from the sinking of brine-enriched waters formed over the shelves [*Dittmar*, 2004]. The remaining fraction (~34 to 50%) should accumulate or be removed by biological and photochemical processes in the Polar Surface Water (PSW). The relative importance for the removal of tDOC by microbial and photochemical processes is unknown [*Amon*,

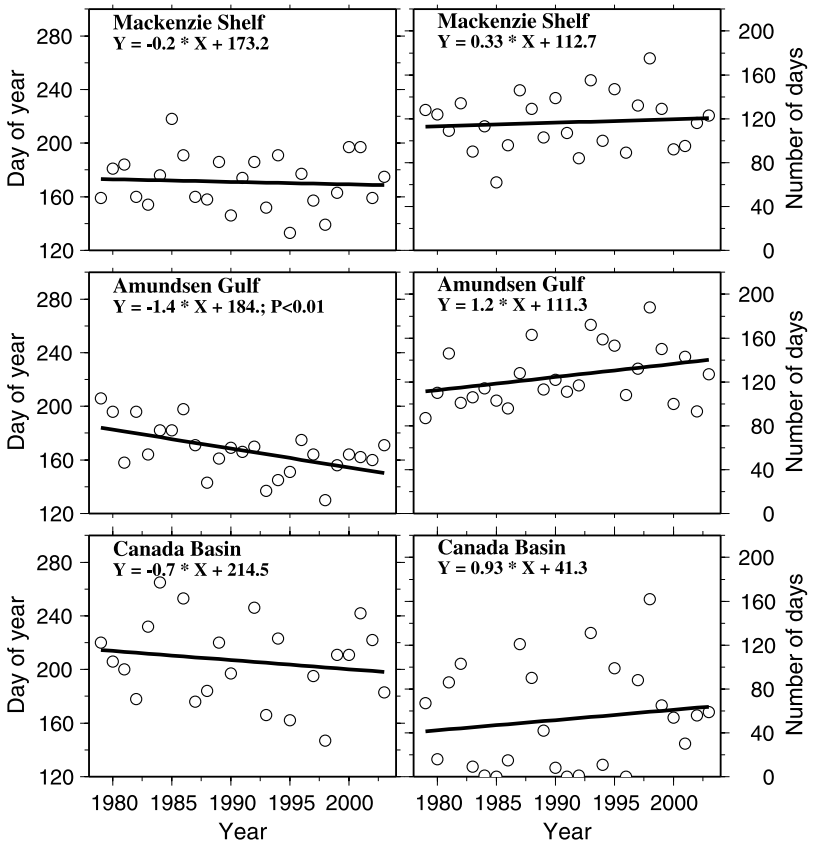

Figure 8. Trends in open water area for the three subregions as observed by SMMR/SSMI between 1979 and 2003. (left) Day of the year when >50% of the surface area is ice free. (right) Number of days having open water.

2004]. Our study is a first attempt to quantify the photochemical sink of tDOC in an Arctic coastal environment affected by large inputs of terrestrial DOM.

[28] The main source of CDOM in the study area is the terrestrial runoff from the Mackenzie River [*Guay et al.*, 1999; *Guéguen et al.*, 2005]. To estimate tDOM mineralization, one needs to know the fraction of light absorbed by the terrigenous CDOM (a^{ter}_{CDOM}). This fraction (in %) was approximated as

$$\frac{a^{ter}_{CDOM}}{a_{CDOM}} = \left(\frac{6.5f}{6.5f + 0.5(1-f)}\right) \times 100, \qquad (6)$$

where f is the fraction of runoff in the surface layer, and 6.5 and 0.5 are the $a_{CDOM}(330)$ values for the riverine and marine end-members, respectively (Figure 3a). On the basis of conservative estimates for f of ~25% in the MS [*Macdonald et al.*, 1995] and ~8% in the CB [*Macdonald et al.*, 2002], we calculated that 80 and 50% of the a_{CDOM} is of terrigenous origin in the MS and CB, respectively (Table 4). The contribution of a^{ter}_{CDOM} in the Amundsen Gulf is less certain and depends on the surface currents and the autochthonous production of CDOM. Under calm wind conditions, the Mackenzie River plume tends to flow eastward and enter the gulf [*Carmack and Macdonald*, 2002]. However, since PP appears relatively important around Cape Bathurst [*Arrigo and van Dijken*, 2004], we assume that only 20% of the CDOM in the AG is of terrigenous origin. This number represents a typical contribution of tDOC to PSW [*Benner et al.*, 2005]. On the basis of these assumptions, tDOC photomineralization is estimated to be 19.9 ± 4.2, 13.1 ± 5.9 and 2.8 ± 0.7 Gg C yr^{-1} for the MS, CB and AG, respectively (Table 4), representing 1.53 ± 0.32%, 1.0 ± 0.5% and 0.21 ± 0.04% of the tDOC flux into the southeastern Beaufort Sea via the Mackenzie River. Put together, these estimates represent 2.8 ± 0.55% of the annual input of tDOC (1.3 Tg) [*Telang et al.*, 1991]. Therefore our results corroborate the speculation by *Benner et al.* [2005] that photochemical transformation of tDOM occurs in the PSW but that this removal process is a small fraction of the total organic carbon flux.

[29] *Amon and Meon* [2004] suggested that the fate of tDOM under reduced ice cover could become significantly different from the present situation, and our results allow further analysis of this prediction for photomineralization losses. Under the minimal sea ice conditions observed during spring-summer 1998, DIC photoproduction nearly doubled relative to the averaged value for the period from 1979 to 2003 (123.0 versus 66.5 Gg C yr^{-1}, $P < 0.0001$). For comparison, we evaluated the implications of future

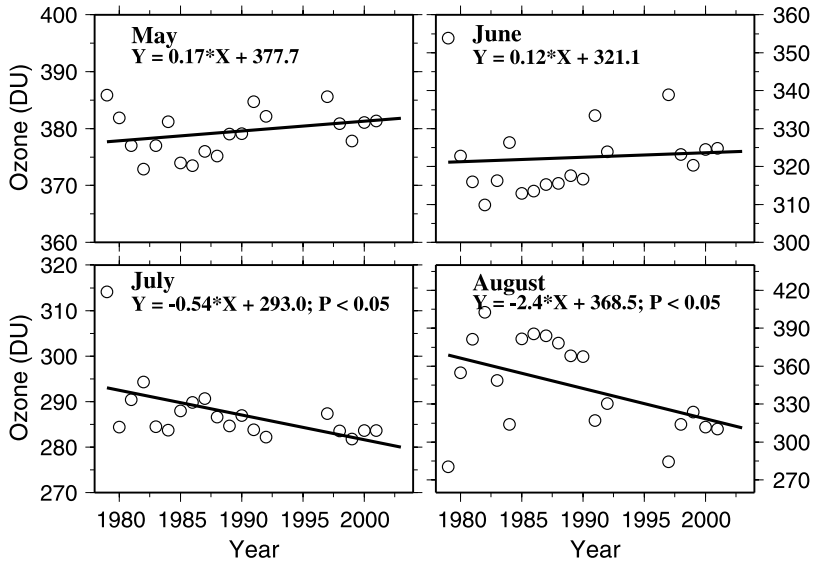

Figure 9. Trends in monthly O_3 concentration over the study area as observed by TOMS between 1979 and 2001. Note the changes of scale among the plots.

summer ice-free conditions. These calculations were based on the following scenario: (1) The opening begins in early April; (2) 50 and 75% of the area is open in early and mid-May, respectively; and (3) the area is totally ice-free from early June to mid-October. Under these conditions, we estimated that 150.5 Gg DIC yr^{-1} would be produced, which is only 22.4% higher than the value estimated for the warm year 1998. Thus future DIC photoproduction rates would not be greatly above that achieved already in warm years. However, this estimate is 2.26 times the mean value for 1979–2003, and photoproduction would routinely persist at this high rate each year under this ice-free scenario.

[30] In September 1997, an abundant amount of Mackenzie River runoff (10 to 25%) entered the surface layer (<40 m deep) of the CB as far as 150°W and 76°N [*Macdonald et al.*, 2002]. Satellite observations in July 1998 confirmed that the river plume extended over large areas of open water created by reduced sea ice cover in the CB [*Macdonald et al.*, 2002]. Consequently, the plume was exposed to UV radiation for longer periods of time thus allowing more tDOC to be photochemically mineralized. On the basis of the relative importance of terrigenous CDOM assumed for each sub-region (Table 4), we estimated 30.0, 32.5 and 4.2 Gg yr^{-1} of tDOC to be photomineralized in 1998 in the MS, CB, and AG respectively, the sum of these numbers representing 5.1% of the annual tDOC release from the Mackenzie River. The ice-free scenario gives an equivalent estimate of 6.2% (assuming no change in tDOC input). For these conditions, we estimated that 43.5 Gg yr^{-1} of allochthonous DOC would be photomineralized in the Canada Basin, which is higher than the estimates for autochthonous organic carbon sequestered in the deep ocean basin (22.8 to 42 Gg C yr^{-1}). This range is based on the assumptions that 1% of the annual PP is buried in sediments [*Stein and Macdonald*, 2004] and that PP rate ranges from 9.5 to 17.4 g C m^{-2} in the open water of CB [*Lee and Whitledge*, 2005].

[31] In this study, photooxidation of CDOM within or under sea ice was not considered because most of the radiative energy is either backscattered to the atmosphere or absorbed by the freshly produced biogenic material accumulated at the bottom of sea ice. Although photochemical reactions within the organic-rich bottom ice layer is likely to play a role in the marine DOM cycling [*Xie and Gosselin*, 2005], it does not affect the underlying terrigenous DOM. Due to the lack of tDOM data in sea ice [*Amon*, 2004], it is impossible at present to estimate the photomineralization of tDOC in sea ice.

4. Summary and Conclusions

[32] This study represents the first attempt to quantify photomineralization of DOM in an Arctic coastal ecosystem

Table 4. Mean Annual DIC Photoproduction and Estimates of tDOC Mineralized by Photooxidation

Subregion	DIC Photoproduction,[a] Gg C yr^{-1}	$\frac{a_{CDOM}^{ter}}{a_{CDOM}}$, %	tDOC Mineralized,[a] Gg C yr^{-1}
Mackenzie Shelf	24.9 ± 5.2	80	19.9 ± 4.2
Canada Basin	27.8 ± 11.8	50	13.9 ± 5.9
Amundsen Gulf	13.7 ± 3.3	20	2.8 ± 0.7
Total	66.5 ± 18.5		36.6 ± 7.1

[a]Average ± s.d. calculated from 1979 to 2003.

that receives large riverine inputs of terrigenous materials. The quantum yield spectra for DIC photoproduction (ϕ_{DIC}) are the first to be obtained for the Arctic, and among the first for marine waters in general. The nonconservative behavior of ϕ_{DIC} in the freshwater-saltwater transitional zone suggests that the photoreactivity of tDOM transported by Mackenzie River changed when it was mixed into coastal and offshore waters, and/or that marine algae-derived DOM was less photoreactive than tDOM in terms of photoproduction of DIC.

[33] Photomineralization of DOC in the study area, as estimated from DIC photoproduction, occurred at a rate equivalent to ~10% of the bacterial respiration rate and <8% of the new production rate. Photochemical production of DIC in the southeastern Beaufort Sea increased over the period 1979 to 2003, by ~15% overall, in response to the decreasing sea ice extent. Our estimates of tDOC photomineralization confirm that photooxidation presently is not a major removal pathway for tDOM in the Arctic. The photochemical sink for tDOM is, however, anticipated to grow in the future owing to decrease in sea-ice extent as predicted by the Global Circulation Model [*Arctic Climate Impact Assessment*, 2005]. In addition to remineralizing CDOM to CO_2, photolysis also produces biologically labile DOM compounds [e.g., *Kieber et al.*, 1989; *Mopper et al.*, 1991]. The latter may provide another pathway by which Arctic tDOM is removed, thereby amplifying the effect of decrease in sea ice cover on tDOM cycling in the Arctic Ocean.

[34] **Acknowledgments.** This study was made possible with financial support from the Natural Sciences and Engineering Research Council of Canada (NSERC), the Fonds Québécois pour la Recherche sur la Nature et les Technologies (FQRNT) (to HX), and the Fonds France Canada pour la Recherche (FFCR to MB and WFV) and Indian and Northern Affairs Canada (to S. B.). S. B. receives a doctoral fellowship from the FQRNT. We thank S. H. Lee for providing the primary production rates measured in the Gulf of Amundsen. We are grateful to C. Osburn and M. Tzortziou for their constructive comments on the manuscript. We appreciate the efforts of S. Cizmeli in CASES field measurements, T. Lou in DIC measurement and J. Caveen in Matlab programming. We thank the crews of the *CCGS Amundsen* cruises for their enthusiastic help onboard the ship. This is a contribution to the Canadian Arctic Shelf Exchange Study (CASES) under the overall direction of L. Fortier. S. C. Johannessen and one anonymous referee are acknowledged for constructive comments on the manuscript.

References

Aagaard, K., and E. C. Carmack (1989), The role of sea ice and other fresh water in the arctic circulation, *J. Geophys. Res.*, *94*(C10), 14,485–14,498.

Amon, R. M. W. (2004), The role of dissolved organic matter for the organic carbon cycle in the Arctic Ocean, in *The Organic Carbon Cycle in the Arctic Ocean*, edited by R. Stein and R. W. MacDonald, pp. 83–99, Springer, New York.

Amon, R. M. W., and B. Meon (2004), The biogeochemistry of dissolved organic matter and nutrients in two large Arctic estuaries and potential implications for our understanding of the Arctic Ocean system, *Mar. Chem.*, *92*, 311–330.

Arctic Climate Impact Assessment (2005), *Arctic Climate Impact Assessment*, 1042 pp., Cambridge Press Univ., New York.

Arrigo, K. R., and G. L. van Dijken (2004), Annual cycles of sea ice and phytoplankton in Cape Bathurst polynya, southeastern Beaufort Sea, Canadian Arctic, *Geophys. Res. Lett.*, *31*, L08304, doi:10.1029/2003GL018978.

Babin, M., and D. Stramski (2002), Light absorption by aquatic particles in the near-infrared spectral region, *Limnol. Oceanogr.*, *47*, 911–915.

Babin, M., D. Stramski, G. M. Ferrari, H. Claustre, A. Bricaud, G. Obolensky, and N. Hoepffner (2003), Variations in the light absorption coefficients of phytoplankton, nonalgal particles, and dissolved organic matter in coastal waters around Europe, *J. Geophys. Res.*, *108*(C7), 3211, doi:10.1029/2001JC000882.

Barber, D. G., and J. M. Hanesiak (2004), Meteorological forcing of sea ice concentrations in the southern Beaufort Sea over the period 1979 to 2000, *J. Geophys. Res.*, *109*, C06014, doi:10.1029/2003JC002027.

Benner, R., and S. Opsahl (2001), Molecular indicators of the sources and transformations of dissolved organic matter in the Mississippi river plume, *Org. Geochem.*, *32*, 597–611.

Benner, R., B. Benitez-Nelson, K. Kaiser, and R. M. W. Amon (2004), Export of young terrigenous dissolved organic carbon from rivers to the Arctic Ocean, *Geophys. Res. Lett.*, *31*, L05305, doi:10.1029/2003GL019251.

Benner, R., P. Louchouarn, and R. M. W. Amon (2005), Terrigenous dissolved organic matter in the Arctic Ocean and its transport to surface and deep waters of the North Atlantic, *Global Biogeochem. Cycles*, *19*, GB2025, doi:10.1029/2004GB002398.

Camill, P. (2005), Permafrost thaw accelerates in boreal peatlands during late-20th century climate warming, *Clim. Change*, *68*, 135–152.

Carmack, E. C., and R. W. Macdonald (2002), Oceanography of the Canadian Shelf of the Beaufort Sea: A setting for marine life, *Arctic*, *55*, 29–45.

Carmack, E. C., R. W. MacDonald, and S. Jasper (2004), Phytoplankton productivity on the Canadian Shelf of the Beaufort Sea, *Mar. Ecol. Prog. Ser.*, *277*, 37–50.

Cavalieri, D. J., P. Gloersen, and J. Zwally (1990), DMSP SSMI/I daily polar gridded sea ice concentrations, edited by J. A. Maslanik, and J. Stroeve, http://nsidc.org/data/docs/daac/nsidc0081_ssmi_nrt_seaice.gd.html, Natl. Snow and Ice Data Cent., Boulder, Colo.

Cavalieri, D. J., C. L. Parkinson, and K. Y. Vinnikov (2003), Thirty-year satellite record reveals contrasting Arctic and Antarctic decadal sea ice variability, *Geophys. Res. Lett.*, *30*(18), 1970, doi:10.1029/2003GL018031.

Comiso, J. C., J. Yang, H. Susumo, and R. A. Krishfield (2003), Detection change in the Arctic using satellite and in situ data, *J. Geophys. Res.*, *108*(C12), 3384, doi:10.1029/2002JC001347.

Del Vecchio, R., and N. V. Blough (2002), Photobleaching of chromophoric dissolved organic matter in natural waters: Kinetics and modelling, *Mar. Chem.*, *78*, 231–253.

Dittmar, T. (2004), Evidence for terrigenous dissolved organic nitrogen in the Arctic deep sea, *Limnol. Oceanogr.*, *49*, 148–156.

Dittmar, T., and G. Kattner (2003), The biogeochemistry of the river and shelf ecosystem of the Arctic Ocean: A review, *Mar. Chem.*, *83*, 105–120.

Dugdale, R. C., and J. J. Goering (1967), Uptake of new and regenerated forms of nitrogen in primary production, *Limnol. Oceanogr.*, *12*, 196–206.

Fioletov, V. E., M. G. Kimlin, N. Krotkov, L. J. B. McArthur, J. B. Kerr, D. I. Wardle, J. R. Herman, R. Meltzer, T. W. Mathews, and J. Kaurola (2004), UV index climatology over the United States and Canada from ground-based and satellite estimates, *J. Geophys. Res.*, *109*(D22), D22308, doi:10.1029/2004JD004820.

Frey, K. E., and L. C. Smith (2005), Amplified carbon release from vast West Siberian peatlands by 2100, *Geophys. Res. Lett.*, *32*, L09401, doi:10.1029/2004GL022025.

Garneau, M.-È., W. F. Vincent, L. Alonso-Saez, Y. Gratton, and C. Lovejoy (2006), Prokaryotic community structure and hetereotrophic production in a river-influenced coastal arctic ecosystem, *Aquat. Microb. Ecol.*, *42*, 27–40.

Guay, C. K., G. P. Klinkhammer, K. K. Falkner, R. Benner, P. G. Coble, T. E. Whitledge, B. Black, F. J. Bussell, and T. A. Wagner (1999), High-resolution measurements of dissolved organic carbon in the Arctic Ocean by in situ fiber-optic spectrometry, *Geophys. Res. Lett.*, *26*(8), 1007–1010.

Guéguen, C., L. Guo, and N. Tanaka (2005), Distributions and characteristics of colored dissolved organic matter in the western Arctic Ocean, *Cont. Shelf Res.*, *25*, 1195–1207.

Hansell, D. A., D. Kadko, and N. R. Bates (2004), Degradation of terrigenous dissolved organic carbon in the western Arctic Ocean, *Science*, *304*, 858–861.

Herman, J. R., and E. A. Celarier (1997), Earth surface reflectivity climatology at 340–380 nm from TOMS data, *J. Geophys. Res.*, *102*(D23), 28,003–28,011.

Herman, J. R., N. Krotkov, E. Celarier, D. Larko, and G. Labow (1999), Distribution of UV radiation at the Earth's surface from TOMS-measured UV-backscattered radiances, *J. Geophys. Res.*, *104*(D10), 12,059–12,076.

Hernes, P. J., and R. Benner (2003), Photochemical and microbial degradation of dissolved lignin phenols: Implications for the fate of terrigenous dissolved organic matter in marine environments, *J. Geophys. Res.*, *108*(C9), 3291, doi:10.1029/2002JC001421.

Hu, C., F. E. Muller-Karger, and R. G. Zepp (2002), Absorbance, absorption coefficient, and apparent quantum yield: A comment on common ambiguity in the use of these optical concepts, *Limnol. Oceanogr.*, *47*, 1261–1267.

Johannessen, S. C. (2000), A photochemical sink for dissolved organic carbon in the ocean, Ph.D. thesis, Dalhousie Univ., Halifax, N. S., Canada.

Johannessen, S. C., and W. L. Miller (2001), Quantum yield for the photochemical production of dissolved inorganic carbon in seawater, *Mar. Chem.*, *76*, 271–283.

Kieber, D. J., J. McDaniel, and K. Mopper (1989), Photochemical source of biological substrates in sea water: Implications for carbon cycling, *Nature*, *341*, 637–639.

Kieber, R. J., X. Zhou, and K. Mopper (1990), Formation of carbonyl compounds from UV-induced photodegradation of humic substances in natural waters: Fate of riverine carbon in the sea, *Limnol. Oceanogr.*, *35*, 1503–1515.

Krotkov, N. A., P. K. Bhartia, J. R. Herman, V. Fioletov, and J. Kerr (1998), Satellite estimation of spectral surface UV irradiance in the presence of tropospheric aerosols: 1. Cloud-free case, *J. Geophys. Res.*, *103*(D8), 8779–8793.

Krotkov, N. A., J. R. Herman, P. K. Bhartia, V. Fioletov, and Z. Ahmad (2001), Satellite estimation of spectral surface UV irradiance: 2. Effects of homogeneous clouds and snow, *J. Geophys. Res.*, *106*(D11), 11,743–11,759.

Krotkov, N., J. Herman, P. K. Bhartia, C. Seftor, A. Arola, S. Kalliskota, P. Taalas, and I. V. Geogdzhaev (2002), Version 2 total ozone mapping spectrometer ultraviolet algorithm: Problems and enhancements, *Opt. Eng.*, *41*, 3028–3039.

Lee, S. H., and T. R. Whitledge (2005), Primary and new production in the deep Canada Basin during summer 2002, *Polar Biol.*, *28*, 190–197.

Macdonald, R. W., D. W. Paton, E. C. Carmack, and A. Omstedt (1995), The freshwater budget and under-ice spreading of Mackenzie River water in the Canadian Beaufort Sea based on salinity and $^{18}O/^{16}O$ measurements in water and ice, *J. Geophys. Res.*, *100*(C1), 895–919.

Macdonald, R. W., F. A. McLaughlin, and E. C. Carmack (2002), Fresh water and its sources during the SHEBA drift in the Canada Basin of the Arctic Ocean, *Deep Sea Res., Part I*, *49*, 1769–1785.

Madronich, S., and S. Flocke (1999), The role of solar radiation in atmospheric chemistry, in *Handbook of Environmental Chemistry*, edited by P. Boule, pp. 1–26, Springer, New York.

Meon, B., and R. M. W. Amon (2004), Heterotrophic bacterial activity and fluxes of dissolved free amino acids and glucose in the Arctic rivers Ob, Yenisei and the adjacent Kara Sea, *Aquat. Microb. Ecol.*, *37*, 121–135.

Miller, W. L., and R. G. Zepp (1995), Photochemical production of dissolved inorganic carbon from terrestrial organic matter: Significance to the oceanic carbon cycle, *Geophys. Res. Lett.*, *22*(4), 417–420.

Mopper, K., and D. J. Keiber (2002), Photochemistry and the cycling of carbon, sulfur, nitrogen and phosphorus, in *Biogeochemistry of Marine Dissolved Organic Matter*, edited by D. A. Hansell and C. A. Carlson, pp. 455–507, Elsevier, New York.

Mopper, K., X. Zhou, R. J. Keiber, D. J. Keiber, R. J. Sikorski, and R. D. Jones (1991), Photochemical degradation of dissolved organic carbon and its impact on the oceanic carbon cycle, *Nature*, *353*, 60–62.

Overland, J. E., M. C. Spillane, and N. N. Soreide (2004), Integrated analysis of physical and biological Pan-Arctic change, *Clim. Change*, *63*, 291–322.

Peterson, B. J., R. M. Holmes, J. W. McClelland, C. J. Vorosmarty, R. B. Lammers, A. I. Shiklomanov, and S. Rahmstorf (2002), Increasing river discharge to the Arctic Ocean, *Science*, *298*, 2171–2173.

Rachold, V., H. Eicken, V. V. Gordeev, M. N. Grigoriev, H.-W. Hubberten, A. P. Lisitzin, V. P. Shevchenko, and L. Schirrmeister (2004), Modern terrigenous organic carbon input to the Arctic Ocean, in *The Organic Carbon Cycle in the Arctic Ocean*, edited by R. Stein and R. W. MacDonald, pp. 33–41, Springer, New York.

Rex, M., R. J. Salawitch, P. von der Gathen, N. R. P. Harris, M. P. Chipperfield, and B. Naujokat (2004), Arctic ozone loss and climate change, *Geophys. Res. Lett.*, *31*, L04116, doi:10.1029/2003GL018844.

Rothrock, D. A., and J. Zhang (2005), Arctic Ocean sea ice volume: What explains its recent depletion?, *J. Geophys. Res.*, *110*, C01002, doi:10.1029/2004JC002282.

Serreze, M. C., J. E. Walsh, F. S. Chapin, T. Osterkamp, M. Dyurgerov, V. Romanovsky, W. C. Oechel, J. Morison, T. Zhang, and R. G. Barry (2000), Observational evidence of recent change in the northern high-latitude environment, *Clim. Change*, *46*, 159–207.

Smith, L. C., G. M. MacDonald, A. A. Velichko, D. W. Beilman, O. K. Borisova, K. E. Frey, K. V. Kremenetski, and Y. Sheng (2004), Siberian peatlands a net carbon sink and global methane source since the early Holocene, *Science*, *303*, 353–356.

Stein, R., and R. W. Macdonald (2004), Organic carbon budget: Arctic Ocean vs. Global Ocean, in *The Organic Carbon Cycle in the Arctic Ocean*, edited by R. Stein and R. W. MacDonald, pp. 315–322, Springer, New York.

Tassan, S., and G. M. Ferrari (1995), An alternative approach to absorption measurements of aquatic particles retained on filters, *Limnol. Oceanogr.*, *40*, 1358–1368.

Tassan, S., and G. M. Ferrari (2002), A sensitivity analysis of the 'transmittance-reflectance' method for measuring light absorption by aquatic particles, *J. Plankton Res.*, *24*, 757–776.

Telang, S. A., R. Pocklington, A. S. Naidu, E. A. Romankevich, I. I. Gitelson, and M. I. Gladyshev (1991), Carbon and mineral transport in major North American, Russian Arctic, and Siberian rivers: The St Lawrence, the Mackenzie, the Yukon, the Arctic Alaskan rivers, the Arctic Basin rivers in the Soviet Union, and the Yenisei, in *Biogeochemistry of Major World Rivers: SCOPE 42*, edited by E. T. Degens, S. Kempe, and J. E. Richey, pp. 74–104, John Wiley, Hoboken, N. J.

Vähätalo, A. V., and R. G. Wetzel (2004), Photochemical and microbial decomposition of chromophoric dissolved organic matter during long (months-years) exposures, *Mar. Chem.*, *89*, 313–326.

Vähätalo, A. V., M. Salkinoja-Salonen, P. Taalas, and K. Salonen (2000), Spectrum of the quantum yield for the photochemical mineralization of dissolved organic carbon in a humic lake, *Limnol. Oceanogr.*, *45*, 664–676.

Vincent, W. F., and C. Belzile (2003), Biological UV exposure in the polar oceans: Arctic-Antarctic comparisons, in *Antarctic Biology in a Global Context*, edited by W. J. Wolff, pp. 176–181, Backhuys, Leiden, Netherlands.

Wadhams, P., and N. R. Davis (2000), Further evidence of ice thinning in the Arctic Ocean, *Geophys. Res. Lett.*, *27*(24), 3973–3975.

Xie, H., and M. Gosselin (2005), Photoproduction of carbon monoxide in first-year sea ice in Franklin Bay, southeastern Beaufort Sea, *Geophys. Res. Lett.*, *32*, L12606, doi:10.1029/2005GL022803.

Xie, H., O. C. Zafiriou, W.-J. Cai, R. G. Zepp, and Y. Wang (2004), Photooxidation and its effects on the carboxyl content of dissolved organic matter in two coastal rivers in the southeastern United States, *Environ. Sci. Technol.*, *38*(15), 4113–4119.

M. Babin and S. Bélanger, Université Pierre et Marie Curie-Paris6, Laboratoire d'océanographie de Villefranche, F-06230 Villefranche-sur-Mer, France. (marcel@obs-vlfr.fr; sbe@obs-vlfr.fr)

N. Krotkov, Goddard Earth Sciences and Technology Center, University of Maryland Baltimore County, Baltimore, MD 21250, USA. (krotkov@chescat.gsfc.nasa.gov)

P. Larouche, Institut Maurice-Lamontagne, Pêches et Océans Canada, Mont-Joli, QC, Canada G5H 3Z4, (larouchep@dfo-mpo.gc.ca)

W. F. Vincent, Département de Biologie and Centre d'Études Nordiques, Université Laval, Quebec City, Quebec, Canada, G1K 7P4, (warwick.vincent@bio.ulaval.ca)

H. Xie, Institut des Sciences de la Mer de Rimouski, Université du Québec à Rimouski, Rimouski, Quebec, Canada G5L 3A1, (huixiang_xie@uqar.qc.ca)